scientific reports

Check for updates

OPEN

Development and validation of a predictive model based on β-Klotho for head and neck squamous cell carcinoma

XiangXiu Wang[1,2,5], HongWei Liu[3,5], Gang Wu[4], Yan Lu[2] & Ying Cui[2]✉

Head and neck epithelial tissue tumors may be identified as head and neck squamous cell carcinoma (HNSC). Numerous malignancies are encouraged by dysregulation of the FGF19-β-Klotho (KLB) axis in the tumor microenvironment. Using protein databases and RT-qPCR, we examined KLB expression in HNSC. In HNSC, higher KLB expression was linked to longer survival times and better prognoses. Furthermore, variations in drug susceptibility and immunological infiltration were noted according to KLB expression levels. These results underscore the importance of KLB in the course and management of HNSC by indicating that it may function as a possible prognostic marker and influence immunological and therapeutic responses in these individuals. Further study on HNSC is necessary to investigate KLB's potential as a therapeutic target and prognostic indicator.

Head and neck squamous cell carcinoma (HNSC) originates from the mucosal epithelial cells of the oral cavity, pharynx, larynx, and sinuses[1]. It is a highly aggressive and heterogeneous tumor. Most patients diagnosed with HNSC had no history of premalignant lesions[2]. HNSC had 870,000 cases and 440,000 new deaths worldwide in 2020[3]. Although immune checkpoint inhibitors have been approved by the US Food and Drug Administration for the treatment of cisplatin-refractory relapsed or metastatic HNSC[4], to overcome the barriers of targeted therapy and prolong the survival of patients, further studies on detailed molecular characterization and prognostic signatures are still needed.

Over the past decades, research has emphasized the tumor microenvironment's important role in developing head and neck cancer progression. The tumor microenvironment of HNSC consists of complex cellular and non-cellular components. The cellular features include cancer-associated fibroblasts, endothelial cells, adipocytes, immune cells, etc., and the noncellular components include ECM proteins and physicochemical indicators[5]. Extracellular matrix (ECM) is an essential component of the tumor microenvironment, and its interaction with the tumor microenvironment influences tumor progression[6]. Previous studies have shown that dysregulated FGF/FGFR signaling is associated with a non-T-cell inflammatory phenotype in tumors.

In contrast, inhibition of FGFR signaling in HNSC upregulates IFN-gamma in the TME, thereby promoting T-cell differentiation[7]. The KL gene family was initially identified as being associated with anti-aging[8] and is strongly associated with aging-related diseases. β-klotho (KLB) is a single transmembrane protein. KLB binds to FGFR1c to form the receptor for FGF21[9], and KLB binds to FGFR4 to form the receptor for FGF19[10]. It has been shown that the Klotho-FGF endocrine axis is closely associated with aging-related diseases, including tumors[11,12]. However, KLB's role in the HNSC tumor microenvironment remains to be further investigated.

We examined the transcriptome data of HNSC in the TCGA. We discovered a significant trend of decreasing KLB expression levels in tumor samples compared to standard samples, as well as that patients with high KLB expression in tumor samples had more prolonged survival than patients with low KLB expression. As a result, the current work aims to investigate the particular role of KLB in the HNSC tumor microenvironment and to correlate it with clinical indicators to predict the prognosis of HNSC patients and the effect of immunotherapy based on KLB and its related gene expression levels.

[1]Jinzhou Medical University, Jinzhou 121000, China. [2]Department of Otorhinolaryngology, The First Affiliated Hospital of Jinzhou Medical University, Jinzhou 121000, China. [3]Cancer Hospital of China Medical University, Shenyang 110042, China. [4]Department of Hepatobiliary Surgery, The First Affiliated Hospital of Jinzhou Medical University, Jinzhou 121000, China. [5]These authors contributed equally: XiangXiu Wang and HongWei Liu. ✉email: yingwuwu2002@jzmu.edu.cn

Results

KLB is lowly expressed in tumor tissue

Figure 1 illustrates the study flow. To determine whether KLB plays a role in human cancers, we first examined the expression of the KLB gene in different cancers in the Cancer Genome Atlas (TCGA) database through the database TIMER 2.0. As shown in Fig. 2A, KLB is lowly expressed in 15 epithelial-type tumors compared to standard samples, including Breast invasive carcinoma, Cholangio carcinoma, Colon adenocarcinoma, Glioblastoma multiforme, Thyroid carcinoma, Kidney chromophobe, Kidney renal clear cell carcinoma, Kidney renal papillary cell carcinoma, Liver hepatocellular carcinoma, Lung adenocarcinoma, Lung squamous cell carcinoma, Prostate adenocarcinoma, Rectum adenocarcinoma, Stomach adenocarcinoma, and Head and Neck Squamous Cell Carcinoma. We compared the expression of KLB in HNSC with that of normal samples, and the results in Fig. 2B,C show that KLB is lower expressed in HNSC. In addition, Fig. 2E–H shows the immunohistochemical staining results of the HNSC tumor and paraneoplastic tissues, with KLB expressed at low levels in tumor tissue.

To validate the results of bioinformatics analysis, we selected pathological specimens of cancerous (n = 8) and paraneoplastic (n = 8) tissues from patients with squamous cell carcinoma of the head and neck and extracted total tissue RNA. We analyzed the relative expression of KLB in cancerous and paraneoplastic tissues using the RT-qPCR method. The outcomes showed that the word of KLB was significantly lower in cancer tissues than in the paraneoplastic tissues, consistent with the bioinformatics analysis (Fig. 2D).

KLB expression correlates with immune infiltration

Next, we assessed the relationship between KLB expression and immune infiltration using the CIBERSORT algorithm. As shown in Fig. 3A–H, the transcriptional expression of KLB was negatively correlated with Mast cells activated, Macrophages M2, Macrophages M0, and NK cells resting, and positively correlated with T cells regulatory (Tregs), T cells follicular helper, T cells CD8, Plasma cells and B cells naïve. On the other hand, KLB highly expressing HNSC patients with B cells naive, Plasma cells, T cells follicular helper and T cells regulatory (Tregs) high infiltration and NK cells resting, Macrophages M0 and Macrophages M2 low infiltration (Fig. 3I).

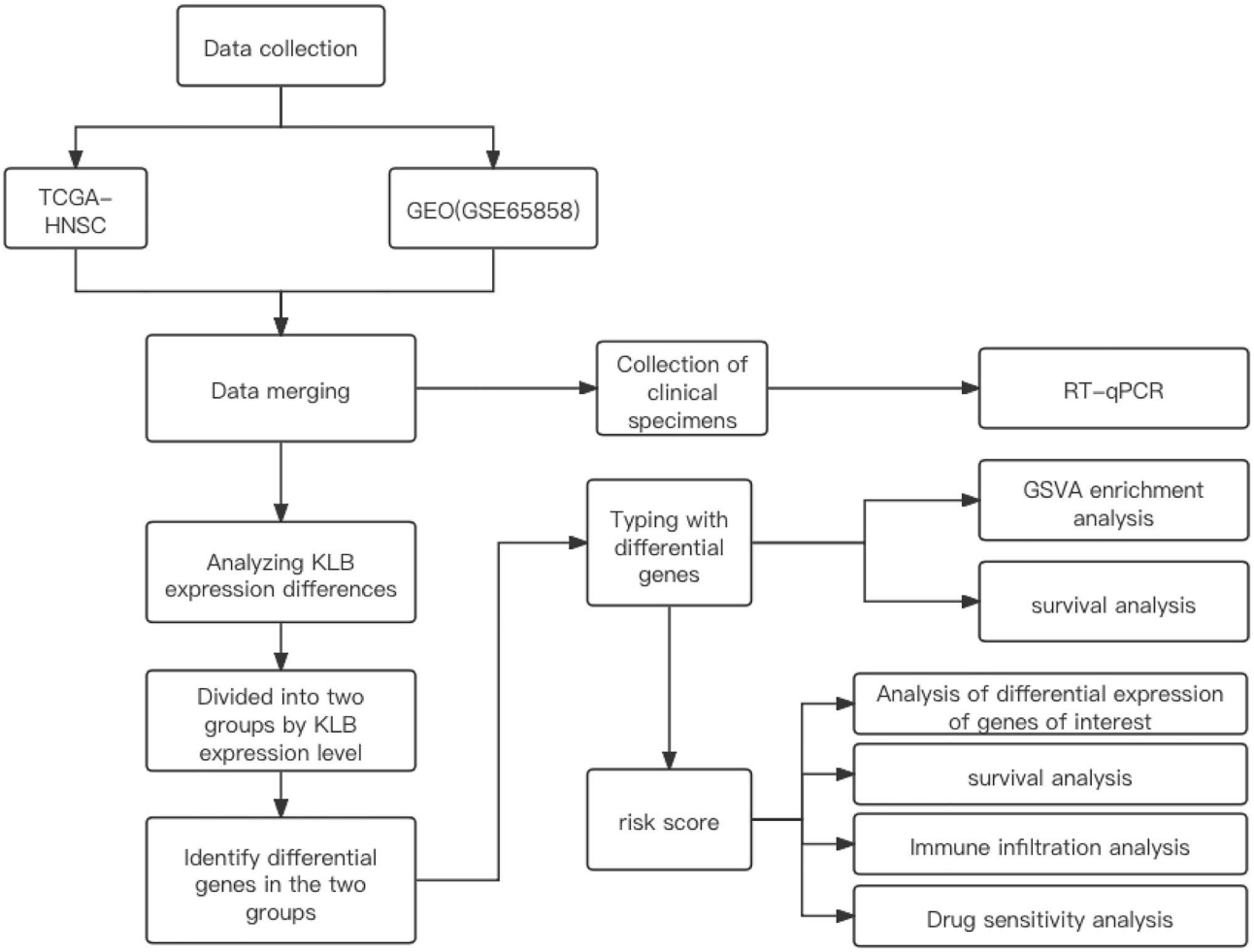

Figure 1. The whole analytical process of the study.

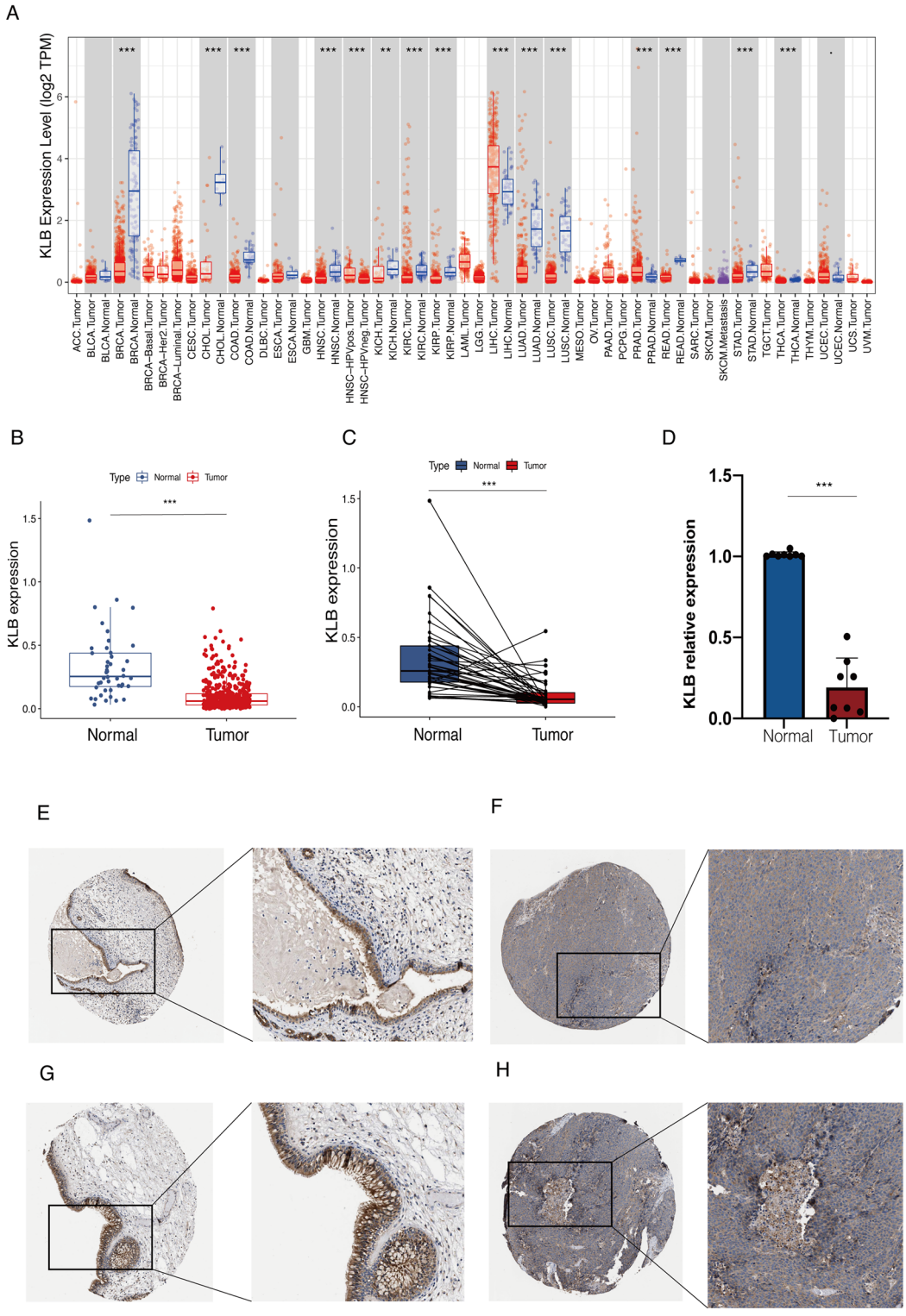

Figure2. Differences in KLB expression between tumor and paraneoplastic tissues. (**A**) KLB expression in pan-cancer. (**B**) KLB expression was lower in tumor tissues than in paraneoplastic tissues in TCGA-HNSC data. (**C**) Lower KLB expression in tumor tissues than paraneoplastic tissues in paired samples of TCGA-HNSC data. (**D**) In collected clinical samples, there was a higher KLB expression in paraneoplastic tissues (N = 8) than in tumor tissues (N = 8). (**E**–**H**) Immunohistochemical staining of head and neck tissues against KLB expression levels in the HPA database. (**F**) and (**H**) are from different parts of sections from the same patient, and (**E**) and (**G**) are from different patients' normal mucosal epithelial tissues of the head and neck. (**E**) Specimen number HPA021136, site: head and neck normal tissue, patient id: 3362, (**F**) Specimen number HPA021136, site: head and neck, squamous carcinoma tissue, patient id: 2547, (**G**) Specimen number HPA021136, site: head and neck, normal nasopharyngeal tissue, patient id: 3402, (**H**) Specimen number HPA021136, site: head and neck, head and neck, squamous carcinoma tissue, patient id: 2547).

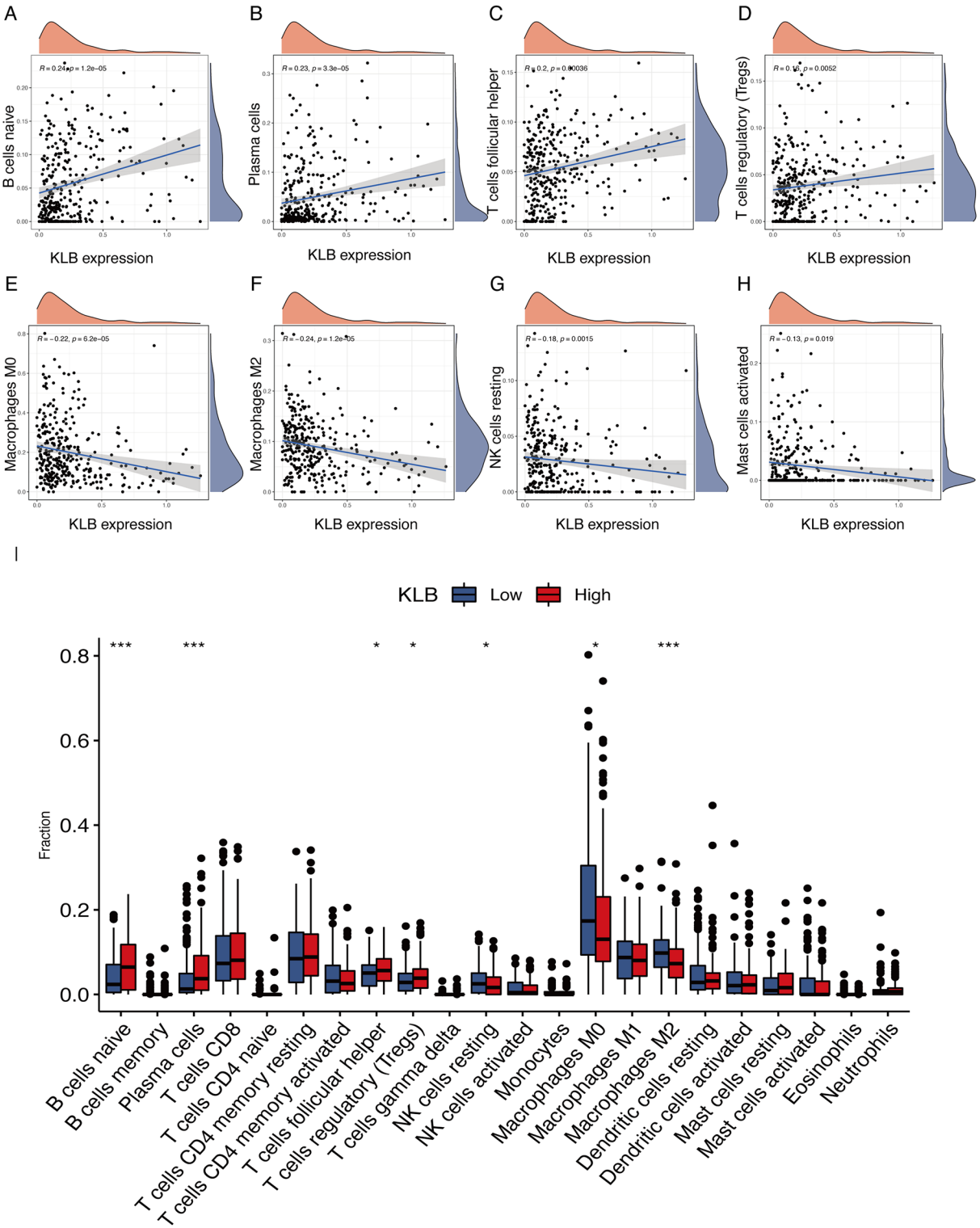

Figure 3. Relationship between KLB expression level and immune infiltration. (**A–H**) The transcriptional expression of KLB was negatively correlated with Mast cells activated, Macrophages M2, Macrophages M0, and NK cells resting, and positively correlated with T cells regulatory (Tregs), T cells follicular helper, T cells CD8, Plasma cells and B cells naïve. (**I**) Differences in immune cell infiltration between KLB high and low expression groups.

Correlation of KLB expression with the prognosis of HNSC patients

To investigate the prognostic value of KLB in HNSC, we used the Kaplan–Meier Plotter to predict the relationship

between KLB expression and the overall survival of HNSC patients. Figure 4A showed a significant difference between the high and low KLB expression groups. Median survival was higher in the high KLB expression group than in the low KLB expression group, which indicated that KLB expression might be associated with a better prognosis for HNSC patients. In addition, we compared the impact of KLB on overall survival in male and female patients separately. The overall survival rate was higher in male patients with higher KLB expression than in patients with lower KLB expression. In contrast, there was no statistically significant difference in the effect of KLB on overall survival in female patients (Fig. 4B,C).

To further investigate the prognostic value of KLB, we merged HNSC transcriptomic and clinical data from TCGA (normal = 44, tumor = 500) and a GEO dataset containing HNSC transcriptomic expression data and survival time and survival status (GSE65858, n = 270). We divided the 772 HNSC samples into a KLB high-expression group and a KLB low-expression group. We found the differential genes between the two groups, with the screening criteria of $P < 0.05$ and Log FC > 1 (Fig. 4D). We found 2798 genes that differed between groups and used the R package "Consensus Cluster Plus" to cluster all HNSC samples based on the expression patterns of the differential genes. The clustering was best when all samples were divided into three subtypes with good intra-subtype stability. We named the KLB subtypes A–C, with KLB cluster A containing 281 illustrations, KLB cluster B containing 409 samples, and KLB cluster C collecting 82 samples. Survival analysis showed that samples in cluster C had a better prognosis than those in clusters A and B (Fig. 4E). In addition, we used GSEA analysis to explore the internal characteristics of the three subtypes. We obtained enrichment analysis results showing that C subtypes are associated with immune activation, such as the Fc epsilon RI signaling pathway, B cell receptor signaling pathway, T cell receptor signaling pathway, the intestinal immune network for Ig A production, and natural killer cell-mediated cytotoxicity. In contrast, the B subtype is associated with pathways that promote tumor progression, such as the Wnt signaling pathway (Fig. 4F,G). In addition, immune cell infiltration-related pathways, such as the B cell receptor signaling pathway, T cell receptor signaling pathway, and natural killer cell-mediated cytotoxicity, were up-regulated in the A subtype compared to the B subtype.

Prognostic risk assessment of HNSC patients using differential genes grouped by KLB expression

To assess the prognostic risk of HNSC patients, we performed unifactorial Cox analysis on differential genes grouped by KLB expression to find prognosis-related genes; all samples were randomly divided into a training set and a test set and then performed lasso regression analysis and multifactorial Cox regression analysis on these prognosis-related genes to finally obtain 16 genes for assessing the KLB-Related Prognostic Risk Score (KRPRS) of HNSC patients. Eight of these positive factors were: ODF4, FAM187B, RAB37, CALN1, SRY, PLA2G2D, PIWIL2, CALML5 and eight negative factors were: TRIML2, KIF1A, SRPX, DPY19L2P1, CDKL2, RLN2, TMEFF2, C4BPB. The KLB-Related Prognostic Risk Score = expression level of ODF4*(− 1.135722681) + FAM187B*(-1.12696817) + RAB37*(− 0.494219462) + CALN1*(− 0.364682077) + SRY*(-0.324556358) + PLA2G2D*(− 0.220799715) + PIWIL2*(− 0.175252875) + CALML5*(− 0.060812431) + TRIML2*0.141813192 + KIF1A*0.16220514 + SRPX*0.178929297 + DPY19L2P1*0.428554182 + CDKL2*0.436786829 + RLN2*0.703418091 + TMEFF2*0.779739064 + C4BPB*1.317576808.Taking the median KRPRS as the cutoff value, in both the training and validation sets, the high KLB-Related Prognostic Risk Score group had a poorer prognosis than the low KRPRS group. We also analyzed the difference in KLB expression between the high-risk and low-risk groups. We showed that KLB expression was lower in the high-risk group (Fig. 5A), suggesting that lower KLB expression predicted a higher risk score and a worse prognosis. The results of the ROC analysis show that the area under the curve at 1, 3, and 5 years is above 0.65 (Fig. 5B). The conclusions we obtained in the training and test sets are consistent.

The low-risk score group had higher PD-L1 expression and immune cell infiltration

To explore the differences between the high and low-risk score groups, we compared the differences in immune cell infiltration between the high and low-risk groups. Previous accumulating evidence suggests that high tumor mutation load implies durable anti-PD-1/PD-L1 immunotherapy; we compared the differences in PD-1 and PD-L1 expression between the high-risk and low-risk groups and showed that PD-L1 expression was higher in the low-risk group compared to the high-risk group (Fig. 5C,D). Therefore, the above results indirectly demonstrate that risk scores predict clinical response to anti-PD-1/PD-L1 immunotherapy. In addition, the results showed that the high-risk score group had higher Macrophages M0, Mast cells activated, and T cells CD4 memory resting infiltration. The low-risk score group had higher Macrophages M1, T cells CD4 memory started, T cells CD8, T cells follicular helper, T cells gamma delta, T cells regulatory (Tregs), and B cells naïve infiltration (Fig. 5E). Next, we analyzed high- and low-risk scores for tumor mutations in the TCGA-HNSC cohort using the map tools package. Figure 5F,G shows that the high-risk score group predicted a higher tumor mutation load than the low-risk score.

Evaluation of response to drug candidates in patients at high and low risk of HNSC

To calculate drug sensitivity for each sample of patients in the high-risk and low-risk groups, we used the R package pRRophetic to identify 73 compounds that differed between the high-risk and low-risk scoring groups. The five drugs with the strongest positive correlation between risk score and drug sensitivity were ATRA(R = 0.49), THZ-2-49(R = 0.47), KIN001-102(R = 0.45), GSK690693(R = 0.36), MK-2206(R = 0.36) (Fig. 6A–J). Of these, ATRA (trans-retinoic acid), THZ-2-49 (selective CDK7 inhibitor), KIN001 (a patented drug combination of Pamapimod and pioglitazone, two active ingredients of an oral drug), GSK690693 (Pan-Akt inhibitor), and MK-2206, a selective Akt1/2/3 inhibitor. To predict the responsiveness of different risk groups to immune checkpoint inhibitor therapy, TIDE scores and the proportion of samples expected to be "responders" in various risk

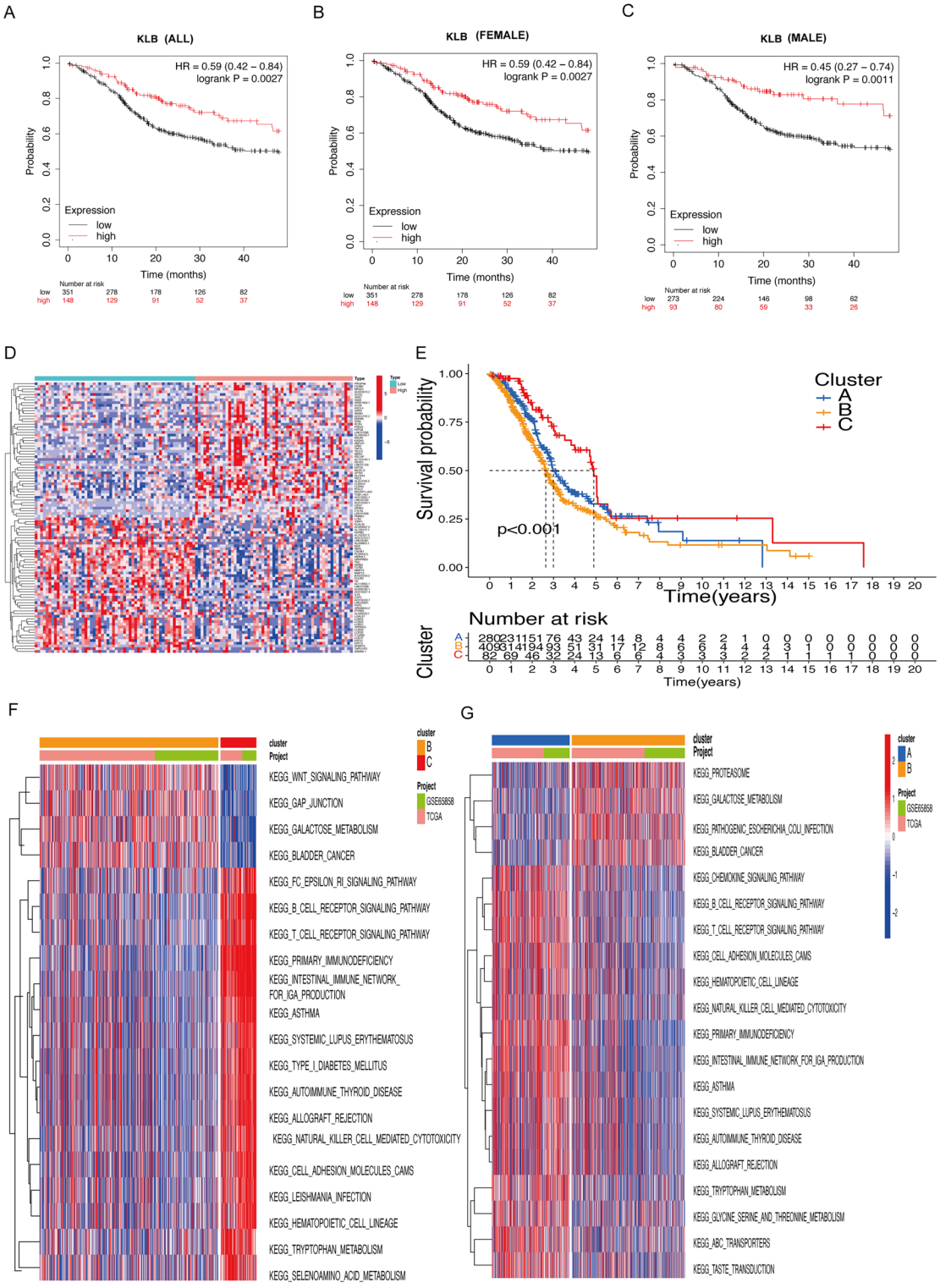

Figure 4. KLB expression levels correlate with survival in HNSC patients. (**A**–**C**). K–M plotter plotted survival curves for HNSC patients, with more prolonged survival in the high KLB expression group in overall and male patients and no statistically significant difference in survival between high and low KLB expression in female patients. (**A**). Survival of different KLB expression subgroups in the overall situation. (**B**) survival of different KLB expression subgroups when sex is female. survival of different KLB expression subgroups when sex is male). (**D**) Differential genes between high and low KLB expression groups. (**E**) Survival differences between the three subtypes. (**F**) and (**G**) Enrichment analysis between the three subtypes. (**F**) Comparative results of enrichment analysis between subtype B and subtype C. Twenty differentially expressed pathways between the two isoforms are illustrated in the figure. (**G**) Comparative results of enrichment analysis between subtype A and subtype B. Twenty differentially expressed pathways between the two isoforms are illustrated in the figure).

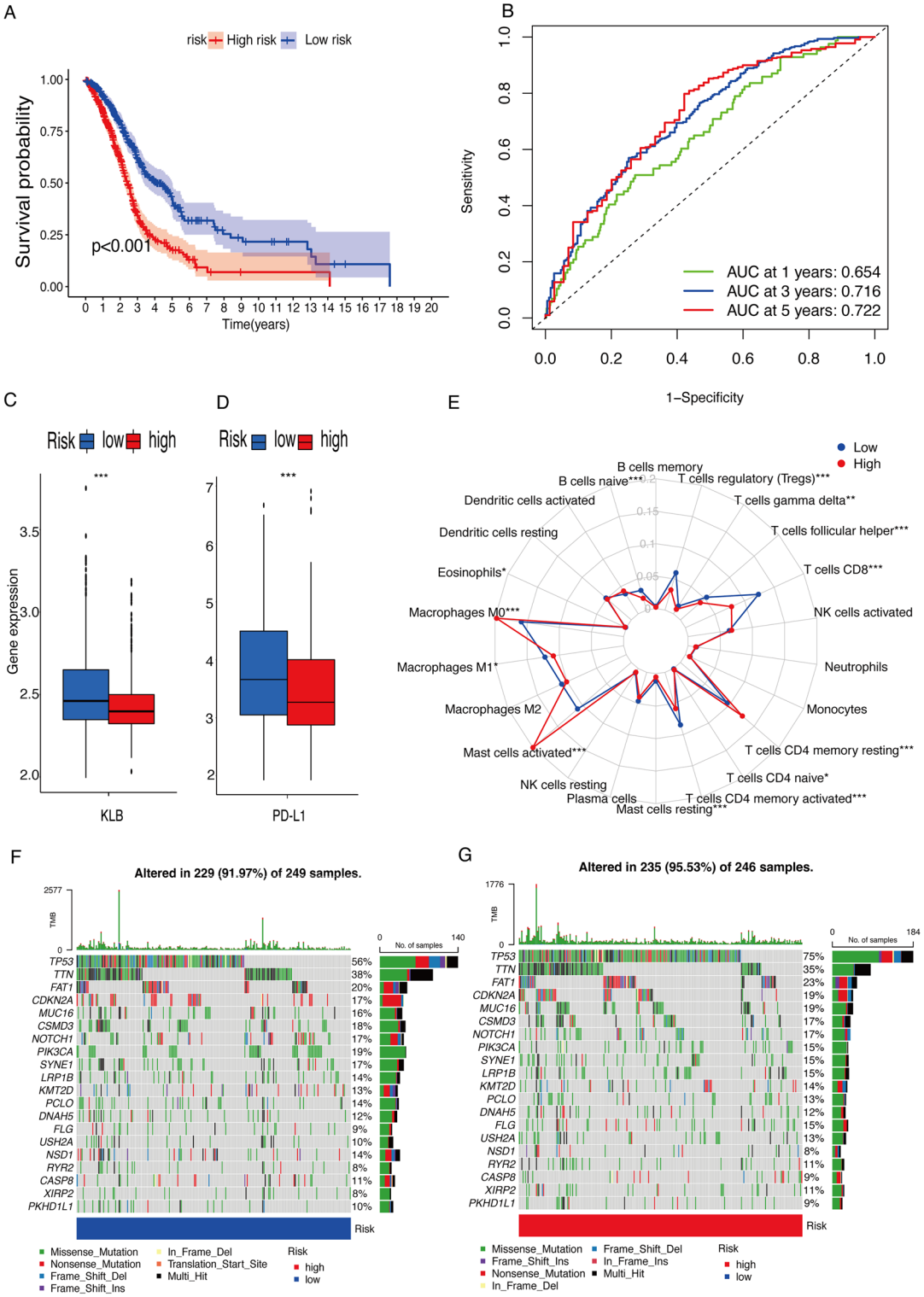

Figure 5. Construction of a prognostic risk score for HNSC patients based on differential genes between the three subtypes. (**A**) Survival differences between high and low-risk groups. (**B**) Accuracy of AUC curves to assess prognostic modeling. (**C**) and (**D**) Difference in expression of KLB, PD-L1 between high and low-risk groups. (**E**) Difference in immune infiltration between high and low-risk groups. (**F**) and (**G**) Mutation differences in transcription factors associated with tumor progression between high and low-risk groups. (F. Waterfall plot of gene mutations in the low-risk group. G. Waterfall plot of gene mutations in high-risk group).

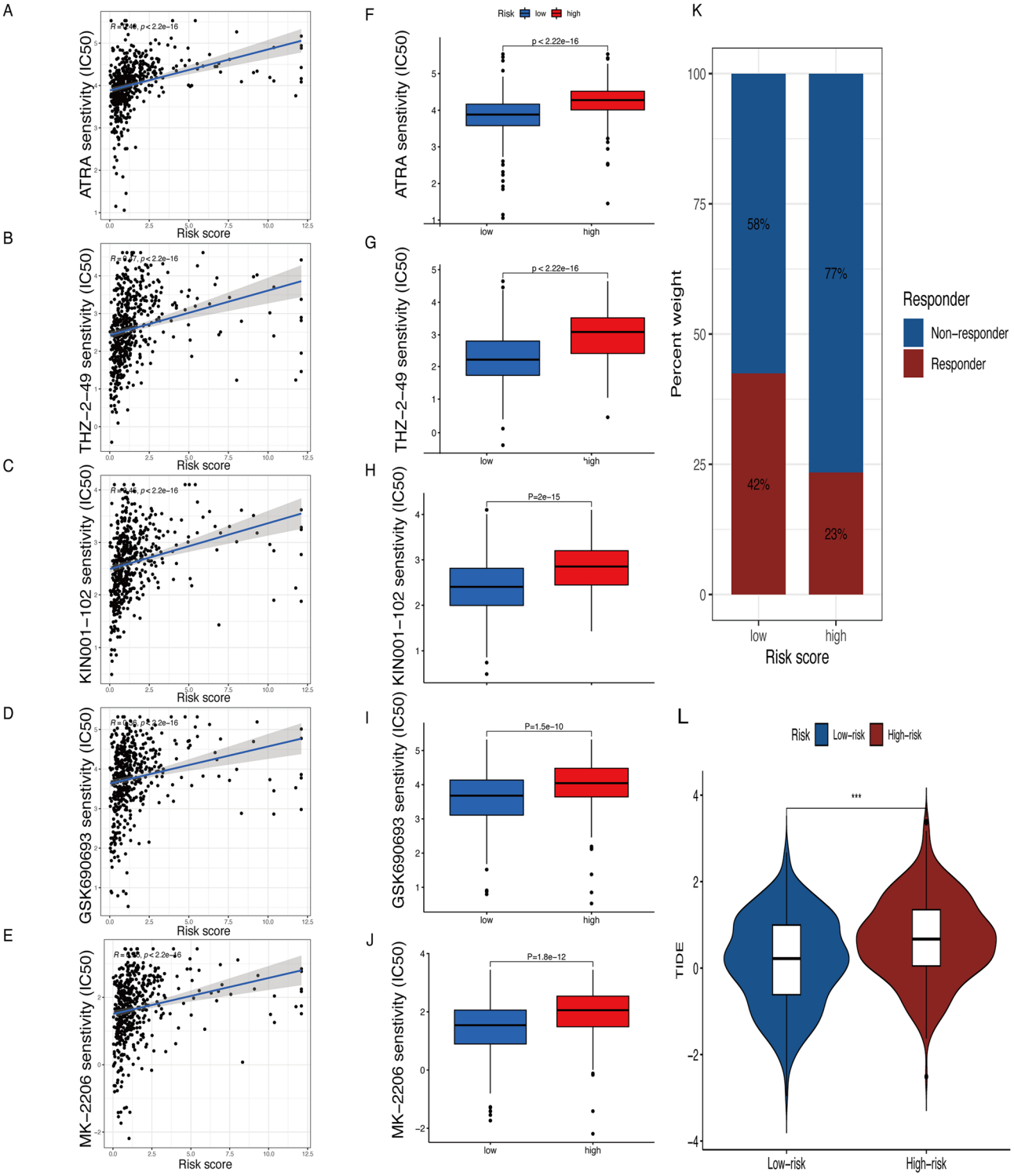

Figure 6. Drug sensitivity analysis between high and low-risk groups. (**A**–**E**) Risk Scores were positively correlated with IC50 for ATRA (R = 0.49), THZ-2-49 (R = 0.47), KIN001-102 (R = 0.45), GSK690693 (R = 0.36), and MK-2206 (R = 0.36). **F**–**J**) HNSC patients in the low-risk group had higher drug sensitivity to ATRA, THZ-2-49, KIN001-102, GSK690693, and MK-2206. K–L. TIDE score for assessing immune checkpoint inhibitor therapy responsiveness in individual tumor patients. (**K**) Percentage of Responder and Non-responder in high and low Risk groups. (**L**) Difference in TIDE scores between high- and low-risk groups).

groups were compared between the high-risk and low-risk groups. The TIDE scores of the low-risk group were significantly lower than those of the high-risk group, and the proportion of "responder" samples in the low-risk

group was higher than that in the high-risk group (Fig. 6K–L). This suggests that the samples in the low-risk group have a better response to immune checkpoint inhibitors.

Discussion

This study found that head and neck squamous cell carcinoma tumor samples had lower KLB expression levels than paraneoplastic tissues. Prognostic models and risk scores for patients with head and neck squamous cell carcinoma were constructed on this basis. KLB expression was low in the high-risk group and high in the low-risk group. Significant differences in the level of immune infiltration, drug sensitivity, and responsiveness to immune checkpoint inhibitor therapy between the high-risk and low-risk groups. In addition, the expression of PD-L1 in the high-risk group was lower than in the low-risk group. The above results suggest that KLB can be used as a prognostic marker and potential target for patients with head and neck squamous cell carcinoma, and the prognostic model constructed with 16 related genes identified with KLB as the core gene can predict the prognosis and immunotherapy effect of patients.

Studies have consistently shown that the expression level of KLB is closely associated with tumor progression[13,14]. Mechanistically, it may be related to the regulatory role of KLB with fibroblast growth factor in the tumor extracellular stroma[15]. KLB as a co-receptor of FGFR4 is involved in the metabolic homeostasis of bile acids, glucose, and lipids in the organism[16], and when the expression level of KLB is decreased in tumor patients, the dynamic equilibrium of the FGFR4-KLB axis of the organism is disrupted, which further activates the pro-cancer effect of FGF19-FGFR4. In addition, it has been demonstrated that KLB overexpression promotes macrophage infiltration by decreasing CSF-1 expression, and macrophage infiltration inhibits the progression of endometrial cancer[17]. In terms of the interaction between tumor cells and immune cells, since CD8+ T-cell infiltration was significantly increased in the low-risk group of HNSC, we hypothesized that high KLB expression could up-regulate the surface antigens of tumors and thus promote the recognition of antigens by CD8+ T-cells and the killing of tumor cells[18]. Differences in immune cell infiltration and corresponding immune cell functions according to the high-risk and low-risk groups are shown in Supplementary Table S10[19]. However, high expression of KLB showed a protective effect in lung cancer and a risk factor in hepatocellular carcinoma[20], which may be related to the different roles of fibroblast growth factors in the tumor microenvironment of different tumor types[21].

This study found that HNSC patients with high KLB expression had a good prognosis, more prolonged survival, and more substantial immune infiltration. Patients with high PD-L1 expression have been shown to have better immunotherapy outcomes[22]. In our study, patients with low prognostic risk scores had high levels of KLB expression concomitant with high PD-L1 expression, suggesting that immunotherapy was more effective in patients in the low-risk group. However, analysis of the correlation between the expression levels of KLB and PD-L1 revealed that there was no significant linear correlation between the two (Supplementary Figure. S1), which may be due to the high heterogeneity of patients with head and neck tumors or the correlation between the expression levels of the two was nonlinear. PD-L1 expression is only predictive of immunotherapy efficacy in a subset of tumor patients, not all of them, so other predictors must be consulted[23]. Therefore, this experiment used the TIDE score to predict the responsiveness of individual samples to immunotherapy. Higher TIDE scores represent patients with poorer responsiveness to immune checkpoint inhibitors. The TIDE score of the low-risk group was significantly lower than that of the high-risk group, suggesting that the low-risk group had better responsiveness to immunotherapy. In addition, a lower TIDE score also represents a more extended survival period after immunotherapy in this sample[24]. However, the specific mechanism of KLB's role in the tumor microenvironment and its effect on immune infiltration require further experimental studies.

HNSC is the seventh most common tumor type in the world, with high heterogeneity and poor prognosis. Immunotherapy is effective for some patients, but still, some patients are poorly treated or develop drug resistance. Our study provides references for finding new targets or adjuvant immunotherapy for treating head and neck tumors. In the following analysis, we will explore what role KLB plays in the tumor microenvironment, probe how KLB affects immune infiltration, and further explain why KLB overexpression prolongs the survival of patients with head and neck tumors.

Methods

Data collection and organization

Gene expression data for HNSC were retrieved from the TCGA-HNSC (including 500 tumor samples and 44 normal samples) and GEO (GSE65858) databases (including 270 tumor samples). The gene expression matrix of the GEO database was collated using platform and probe files. Regions with the same gene name corresponding to different probes were averaged. To obtain the gene expression matrix of the merged HNSC samples, the TCGA-HNSC data and the GSE65858 data were merged using the SVA package.

Analysing differences in KLB expression

Based on the expression data of TCGA-HNSC, we used the LIMMA package to analyze the expression difference of KLB in normal and tumor samples. Paired samples were extracted for difference analysis, and statistical plots were produced using the ggplot2 package.

Immune infiltration analysis

To calculate the immune microenvironment for immune cell infiltration and disease, we used CIBERSORT and performed it 1000 times. The analysis results were visualized using the ggplot2 package and the related extension package ggExtra. Gene expression and immune cell infiltration correlations were performed using Spearman's test. The calculated immune infiltration results are in Supplementary Table S1.

Confirmation of differential genes between groups based on KLB expression

The median value of KLB expression was used to divide into two groups of high and low KLB expression, and the LIMMA package was used to confirm the differential genes between the two groups, with the filtering condition of $|\log_2 FC| > 1$; $P < 0.05$. All the differential genes between the groups are listed in Supplementary Table S2.

Genotyping using intergroup differences and identifying subtype characteristics

Unsupervised cluster typing was done using the Consensus Cluster Plus package, and functional annotation was done for each subtype using GSVA with the functionally annotated gene set from the MsigDB database. The results of the enrichment analyses are presented in Supplementary Tables 3–5. Differences were considered significant at a corrected p-value of < 0.05. Survival analyses were done for the three subtypes using the Survival package, statistical results were visualized using the Survminer package, and differences between survival curves were analyzed using the log-rank test.

Construction of risk assessment models

Lasso regression was done using the GLMNET package to fit a COX proportional risk model to the expression data of the KLB subgroups of the differential genes with the survival data, and the area under the ROC curve was calculated. Candidate genes were selected using multivariate Cox analysis to establish a prognostic risk score in the training set. The prediction time was chosen to be the third year, and the results were output when the training set AUC > 0.65 and the validation set AUC > 0.63. The risk score[25] was calculated as follows:

$$Risk\ score = \Sigma(Expi * Coefi)$$

Coefi and Expi denote each gene's risk coefficient and expression, respectively. Risk scores for all samples are presented in Supplementary Table 6. The median value of the risk score was used to differentiate the samples into high- and low-risk groups, ssGSEA was used to assess the immune cell infiltration, and the Spearmen's test was used to analyze the differences between the high- and low-risk groups. The results of the immune infiltration analysis are presented in Supplementary Table 7.

Chemical reagent

Animal Total RNA Isolation Kit (RE-03011) was purchased from Foregene Co. Chengdu, China; reverse transcription kit (AU341-02) was purchased from Beijing Transgen Biotechnology Co., RT-qPCR MIX (11203ES03) was purchased from Yasen Biotech Co. Wuhan, China.

RT-qPCR

Tissue samples of head and neck tumors were obtained from the Department of Otorhinolaryngology of Jinzhou Medical University, and the experimental procedures complied with the requirements of the Ethics Committee of the First Affiliated Hospital of Jinzhou Medical University, and all experiments were conducted according to the requirements of the Ethics Committee of Jinzhou Medical University. All the participating patients signed informed consent. For RNA extraction, RNA was extracted from 50 mg specimens for reverse transcription and RT-qPCR on a single instrument (ABI QuantStudio 3, USA) according to the manufacturer's instructions. We used GAPDH as an internal reference, 2-ΔΔCt to calculate relative gene expression levels, and GraphPad 9.0 to visualize the data. The primer sequences used are listed in Supplementary Table 8.

Online Database

We used TIMER 2.0 (http://timer.cistrome.org/)[26] to analyze the immune infiltration, and HPA, Human Protein Atlas (proteinatlas. org)[27] to find immunohistochemistry section data of KLB in healthy versus head and neck tumor tissues, K–M Plotter (kmplot.com)[28] to find survival data of HNSC patients associated with KLB expression. For all of the above databases, the search term for the disease is HNSC, and the search term for the gene is KLB. To assess predicting responsiveness to immunosuppressive therapy in individual patients, TIDE scores were calculated for individual samples using the TIDE database (Tumor Immune Dysfunction and Exclusion, tide.dfci.harvard.edu)[29], and input transcriptomic data were normalized according to the website's requirements, TIDE scores for each patient are displayed in Supplementary Table S9.

Data sources

RNA-seq data for HNSC patients from TCGA (https://tcga-data.nci.nih.gov/tcga/) and GEO (GSE65858). KEGG enrichment analysis was performed via https://www.genome.jp/kegg/.

Statistical analysis

Data from RT-qPCR were analyzed using the student's t-test, the Willcox test was used in the R. Kaplan–Meier survival analysis, and log-rank tests were applied to conduct univariate survival analysis. Multivariate survival analyses were performed using Cox regression models. P values < 0.05 were considered statistically significant. The statistical analyses in this study were generated by R-4.2.1.

Data availability

The databases used in this study are all publicly available and can be found in the TCGA database (https://portal.gdc.cancer.gov/) and the GEO (https://www.ncbi.nlm.nih.gov/geo/) database.

Received: 16 January 2024; Accepted: 19 July 2024
Published online: 24 July 2024

References

1. Sánchez-Danés, A. & Blanpain, C. Deciphering the cells of origin of squamous cell carcinomas. *Nat. Rev. Cancer* **18**, 549–561. https://doi.org/10.1038/s41568-018-0024-5 (2018).
2. Johnson, D. E. *et al.* Head and neck squamous cell carcinoma. *Nat. Rev. Dis. Primers* **6**, 92. https://doi.org/10.1038/s41572-020-00224-3 (2020).
3. Sung, H. *et al.* Global Cancer Statistics 2020: GLOBOCAN Estimates of Incidence and Mortality Worldwide for 36 Cancers in 185 Countries. *CA Cancer J. Clin.* **71**, 209–249. https://doi.org/10.3322/caac.21660 (2021).
4. Burtness, B. *et al.* Pembrolizumab alone or with chemotherapy versus cetuximab with chemotherapy for recurrent or metastatic squamous cell carcinoma of the head and neck (KEYNOTE-048): A randomised, open-label, phase 3 study. *Lancet (London, England)* **394**, 1915–1928. https://doi.org/10.1016/S0140-6736(19)32591-7 (2019).
5. Bhat, A. A. *et al.* Tumor microenvironment: an evil nexus promoting aggressive head and neck squamous cell carcinoma and avenue for targeted therapy. *Signal Transduct. Target. Ther.* **6**, 12. https://doi.org/10.1038/s41392-020-00419-w (2021).
6. Huang, J. *et al.* Extracellular matrix and its therapeutic potential for cancer treatment. *Signal Transduct. Target. Ther.* **6**, 153. https://doi.org/10.1038/s41392-021-00544-0 (2021).
7. Ruan, R. *et al.* Unleashing the potential of combining FGFR inhibitor and immune checkpoint blockade for FGF/FGFR signaling in tumor microenvironment. *Mol. Cancer* **22**, 60. https://doi.org/10.1186/s12943-023-01761-7 (2023).
8. Kuro-o, M. *et al.* Mutation of the mouse klotho gene leads to a syndrome resembling ageing. *Nature* **390**, 45–51 (1997).
9. Ogawa, Y. *et al.* BetaKlotho is required for metabolic activity of fibroblast growth factor 21. *Proc. Natl. Acad. Sci. United States Am.* **104**, 7432–7437 (2007).
10. Lin, B. C., Wang, M., Blackmore, C. & Desnoyers, L. R. Liver-specific activities of FGF19 require Klotho beta. *J. Biol. Chem.* **282**, 27277–27284. https://doi.org/10.1074/jbc.M704244200 (2007).
11. Zhang, Y. *et al.* The starvation hormone, fibroblast growth factor-21, extends lifespan in mice. *ELife* **1**, e00065. https://doi.org/10.7554/eLife.00065 (2012).
12. Kenyon, C. J. The genetics of ageing. *Nature* **464**, 504–512. https://doi.org/10.1038/nature08980 (2010).
13. Zhou, J., Ben, S., Xu, T., Xu, L. & Yao, X. Serum β-klotho is a potential biomarker in the prediction of clinical outcomes among patients with NSCLC. *J. Thorac. Dis.* **13**, 3137–3150. https://doi.org/10.21037/jtd-21-798 (2021).
14. Li, P., Zhao, M., Qi, X., Zhu, X. & Dai, J. Downregulation of klotho β is associated with invasive ductal carcinoma progression. *Oncol. Lett.* **14**, 7443–7448. https://doi.org/10.3892/ol.2017.7110 (2017).
15. Feng, S., Dakhova, O., Creighton, C. J. & Ittmann, M. Endocrine fibroblast growth factor FGF19 promotes prostate cancer progression. *Cancer Res.* **73**, 2551–2562. https://doi.org/10.1158/0008-5472.CAN-12-4108 (2013).
16. Li, X., Lu, W., Kharitonenkov, A. & Luo, Y. Targeting the FGF19-FGFR4 pathway for cholestatic, metabolic, and cancerous diseases. *J. Intern. Med.* **295**, 292–312. https://doi.org/10.1111/joim.13767 (2024).
17. Hua, F. & Chen, X. β-Klotho inhibits CSF-1 secretion and delays the development of endometrial cancer. *Cell Cycle* **21**, 2132–2144. https://doi.org/10.1080/15384101.2022.2092180 (2022).
18. Seliger, B. & Massa, C. Immune therapy resistance and immune escape of tumors. *Cancers* **13**, 551. https://doi.org/10.3390/cancers13030551 (2021).
19. Seliger, B. Basis of PD1/PD-L1 therapies. *J. Clin. Med.* **8**, 2168. https://doi.org/10.3390/jcm8122168 (2019).
20. Xia, J. *et al.* Aberrant acetylated modification of FGF21-KLB signaling contributes to hepatocellular carcinoma metastasis through the β-catenin pathway. *Int. J. Oncol.* https://doi.org/10.3892/ijo.2023.5539 (2023).
21. Katoh, M. FGFR inhibitors: Effects on cancer cells, tumor microenvironment and whole-body homeostasis (Review). *Int. J. Mol. Med.* **38**, 3–15. https://doi.org/10.3892/ijmm.2016.2620 (2016).
22. Xu, Y. *et al.* The association of PD-L1 expression with the efficacy of anti-PD-1/PD-L1 immunotherapy and survival of non-small cell lung cancer patients: A meta-analysis of randomized controlled trials. *Transl. Lung Cancer Res.* **8**, 413–428. https://doi.org/10.21037/tlcr.2019.08.09 (2019).
23. Alsaab, H. O. *et al.* PD-1 and PD-L1 checkpoint signaling inhibition for cancer immunotherapy: mechanism, combinations, and clinical outcome. *Front. Pharmacol.* **8**, 561. https://doi.org/10.3389/fphar.2017.00561 (2017).
24. Chang, J. *et al.* Constructing a novel mitochondrial-related gene signature for evaluating the tumor immune microenvironment and predicting survival in stomach adenocarcinoma. *J. Transl. Med.* **21**, 191. https://doi.org/10.1186/s12967-023-04033-6 (2023).
25. Feng, Z. *et al.* Multiparametric immune profiling in HPV- oral squamous cell cancer. *JCI Insight* https://doi.org/10.1172/jci.insight.93652 (2017).
26. Li, T. *et al.* TIMER2.0 for analysis of tumor-infiltrating immune cells. *Nucleic Acids Res.* **48**, W509–W514. https://doi.org/10.1093/nar/gkaa407 (2020).
27. Uhlén, M. *et al.* Proteomics. Tissue-based map of the human proteome. *Science* **347**, 1260419. https://doi.org/10.1126/science.1260419 (2015).
28. Nagy, Á., Munkácsy, G. & Győrffy, B. Pancancer survival analysis of cancer hallmark genes. *Sci. Rep.* **11**, 6047. https://doi.org/10.1038/s41598-021-84787-5 (2021).
29. Fu, J. *et al.* Large-scale public data reuse to model immunotherapy response and resistance. *Genome Med.* **12**, 21. https://doi.org/10.1186/s13073-020-0721-z (2020).

Acknowledgements

We appreciated the technical help from Central Laboratory, The First Hospital of Jilin University, while performing experiments.

Author contributions

X.W. and Y.C. were involved in the conception of the work. X.W. and H.L. searched the literature and extracted the data. X.W. wrote the manuscript and carried out the experiments. G.W. and Y.L. collected and organized the samples. Y.C. revised the manuscript. All authors read and approved the manuscript.

Funding

This project was funded by the Department of Science and Technology of Liaoning Province, Project No. 2023JH2/101300077.

Competing interests

The authors declare no competing interests.

Additional information

Supplementary Information The online version contains supplementary material available at https://doi.org/10.1038/s41598-024-68130-2.

Correspondence and requests for materials should be addressed to Y.C.

Reprints and permissions information is available at www.nature.com/reprints.

Publisher's note Springer Nature remains neutral with regard to jurisdictional claims in published maps and institutional affiliations.